

Genetic and Clinical Correlates of AI-Based Brain Aging Patterns in Cognitively Unimpaired Individuals

Ioanna Skampardoni, MS; Ilya M. Nasrallah, MD, PhD; Ahmed Abdulkadir, PhD; Junhao Wen, PhD; Randa Melhem, MS; Elizabeth Mamourian, MS; Guray Erus, PhD; Jimit Doshi, MS; Ashish Singh, MS; Zhijian Yang, BS; Yuhan Cui, MS; Gyujoon Hwang, PhD; Zheng Ren, MS; Raymond Pomponio, BS; Dhivya Srinivasan, MS; Sindhuja Tirumalai Govindarajan, PhD; Paraskevi Parmpi, MS; Katharina Wittfeld, PhD; Hans J. Grabe, MD; Robin Bülow, MD; Stefan Frenzel, MS; Duygu Tosun, PhD; Murat Bilgel, PhD; Yang An, PhD; Daniel S. Marcus, PhD; Pamela LaMontagne, PhD; Susan R. Heckbert, MD, PhD; Thomas R. Austin, PhD; Lenore J. Launer, PhD; Aristeidis Sotiras, PhD; Mark A. Espeland, PhD; Colin L. Masters, MD; Paul Maruff, PhD; Jurgen Fripp, PhD; Sterling C. Johnson, PhD; John C. Morris, MD; Marilyn S. Alpert, PhD; R. Nick Bryan, MD, PhD; Kristine Yaffe, MD; Henry Völzke, MD; Luigi Ferrucci, MD, PhD; Tammie L.S. Benzinger, MD, PhD; Ali Ezzati, MD; Russell T. Shinohara, PhD; Yong Fan, PhD; Susan M. Resnick, PhD; Mohamad Habes, PhD; David Wolk, MD, PhD; Haochang Shou, PhD; Konstantina Nikita, MD, PhD; Christos Davatzikos, PhD

[+ Supplemental content](#)

IMPORTANCE Brain aging elicits complex neuroanatomical changes influenced by multiple age-related pathologies. Understanding the heterogeneity of structural brain changes in aging may provide insights into preclinical stages of neurodegenerative diseases.

OBJECTIVE To derive subgroups with common patterns of variation in participants without diagnosed cognitive impairment (WODCI) in a data-driven manner and relate them to genetics, biomedical measures, and cognitive decline trajectories.

DESIGN, SETTING, AND PARTICIPANTS Data acquisition for this cohort study was performed from 1999 to 2020. Data consolidation and harmonization were conducted from July 2017 to July 2021. Age-specific subgroups of structural brain measures were modeled in 4 decade-long intervals spanning ages 45 to 85 years using a deep learning, semisupervised clustering method leveraging generative adversarial networks. Data were analyzed from July 2021 to February 2023 and were drawn from the Imaging-Based Coordinate System for Aging and Neurodegenerative Diseases (iSTAGING) international consortium. Individuals WODCI at baseline spanning ages 45 to 85 years were included, with greater than 50 000 data time points.

EXPOSURES Individuals WODCI at baseline scan.

MAIN OUTCOMES AND MEASURES Three subgroups, consistent across decades, were identified within the WODCI population. Associations with genetics, cardiovascular risk factors (CVRFs), amyloid β ($A\beta$), and future cognitive decline were assessed.

RESULTS In a sample of 27 402 individuals (mean [SD] age, 63.0 [8.3] years; 15 146 female [55%]) WODCI, 3 subgroups were identified in contrast with the reference group: a typical aging subgroup, A1, with a specific pattern of modest atrophy and white matter hyperintensity (WMH) load, and 2 accelerated aging subgroups, A2 and A3, with characteristics that were more distinct at age 65 years and older. A2 was associated with hypertension, WMH, and vascular disease-related genetic variants and was enriched for $A\beta$ positivity (ages ≥ 65 years) and apolipoprotein E (APOE) $\epsilon 4$ carriers. A3 showed severe, widespread atrophy, moderate presence of CVRFs, and greater cognitive decline. Genetic variants associated with A1 were protective for WMH (rs7209235: mean [SD] $B = -0.07$ [0.01]; P value = 2.31×10^{-9}) and Alzheimer disease (rs72932727: mean [SD] $B = 0.1$ [0.02]; P value = 6.49×10^{-9}), whereas the converse was observed for A2 (rs7209235: mean [SD] $B = 0.1$ [0.01]; P value = 1.73×10^{-15} and rs72932727: mean [SD] $B = -0.09$ [0.02]; P value = 4.05×10^{-7} , respectively); variants in A3 were associated with regional atrophy (rs167684: mean [SD] $B = 0.08$ [0.01]; P value = 7.22×10^{-12}) and white matter integrity measures (rs1636250: mean [SD] $B = 0.06$ [0.01]; P value = 4.90×10^{-7}).

CONCLUSIONS AND RELEVANCE The 3 subgroups showed distinct associations with CVRFs, genetics, and subsequent cognitive decline. These subgroups likely reflect multiple underlying neuropathologic processes and affect susceptibility to Alzheimer disease, paving pathways toward patient stratification at early asymptomatic stages and promoting precision medicine in clinical trials and health care.

JAMA Psychiatry. 2024;81(5):456-467. doi:10.1001/jamapsychiatry.2023.5599
Published online February 14, 2024.

Author Affiliations: Author affiliations are listed at the end of this article.

Corresponding Author: Christos Davatzikos, PhD, Centre for Biomedical Image Computing and Analytics, University of Pennsylvania, 3700 Hamilton Walk, 7th Floor, Philadelphia, PA 19104 (christos.davatzikos@penncmedicine.upenn.edu).

Aging is associated with complex changes in brain structure and function. Diverse genetic, environmental, and pathologic factors may trigger, aggravate, or protect against pathophysiologic processes that underlie neurodegeneration and its clinical manifestation.¹ These factors may act independently, synergistically, or antagonistically. Common age-associated neuropathologies such as Alzheimer disease (AD) and vascular disease have long preclinical phases when magnetic resonance imaging (MRI) can measure early brain changes.^{2,3} Understanding early brain structural changes may provide prognostic information about susceptibility to or presence of neurodegeneration and inform patient treatment and stratification into clinical trials.

Investigation of heterogeneous brain changes in normal to early pathologic brain aging spectrum requires large and diverse databases, not typical of individual neuroimaging studies. New harmonization methods allow cross-cohort constructive integration of datasets, enabling rich mega-analyses. Additionally, novel artificial intelligence (AI) methods, including deep learning (DL), allow data-driven investigation into subtle patterns of brain change.

Here, we unravel brain structural heterogeneity at cognitively asymptomatic stages and relate it to genetics, lifestyle risk factors, amyloid β (A β), cognitive, and clinical data. We apply an advanced semisupervised DL clustering method based on Generative Adversarial Networks (GAN⁴) called Semi-Supervised Clustering via GANs (Smile-GAN⁵) to a large, diverse data set drawn from 11 neuroimaging studies. We hypothesized that we can identify subgroups of early structural brain variability that will have distinct associations with biomedical measures and trajectories of cognitive decline.

Methods

Imaging-Based Coordinate System for Aging and Neurodegenerative Diseases Data

Data were drawn from the Imaging-Based Coordinating System for Aging and Neurodegenerative Diseases (iSTAGING)⁶⁻⁸ international consortium, a collaborative effort to consolidate neuroimaging, clinical, and cognitive data from more than 39 000 individuals across the adult life span. Here, we included time points from individuals without diagnosed cognitive impairment (WODCI) (eMethods 1 in Supplement 1) aged 45 to 85 years at baseline scan from the following studies: the Alzheimer Disease Neuroimaging Initiative (ADNI), Australian Imaging, Biomarker, and Lifestyle (AIBL) Study, Biomarkers for Older Controls at Risk for Dementia (BIOCARD), Baltimore Longitudinal Study of Aging (BLSA), Coronary Artery Risk Development in Young Adults (CARDIA) study, Open Access Series of Imaging Studies (OASIS), University of Pennsylvania Memory Center cohort (Penn-PMC), Study of Health in Pomerania (SHIP), UK Biobank, Women's Health Initiative Memory Study (WHIMS), and Wisconsin Registry for Alzheimer Prevention (WRAP). The supervisory committee of each study approved its inclusion in this project. The institutional review board of the University of Pennsylvania approved this

Key Points

Question What patterns of morphological brain changes are reproducibly detectable in cognitively unimpaired populations, and what are their genetic, clinical, lifestyle, and cognitive features?

Findings In this multistudy harmonized cohort of 27 402 individuals aged 45 to 85 years without diagnosed cognitive impairment, 3 subgroups of structural brain measures in decade-spanning groups in a data-driven manner were found: 1 typical and 2 accelerated aging subgroups, displaying distinct associations with genetics, cognitive decline, cardiovascular risk factors, and amyloid pathology.

Meaning Three genetically distinct and longitudinally stable subgroups display brain changes reflecting differential susceptibility to Alzheimer disease and other neurodegenerative diseases, cognitive decline, and clinical progression.

project. Participants self-identified with the following race and ethnicity categories: Asian, Black, White, and other, which included Hispanic or Latino, multiracial, Native American, unknown, or other. Information about race and ethnicity is presented as given in the originating studies. Race and ethnicity information was presented only to describe the study sample description; it was not considered in the analysis.

All participants gave written informed consent to each study for data acquisition and analyses according to the Declaration of Helsinki. This study followed the Strengthening the Reporting of Observational Studies in Epidemiology (STROBE) reporting guidelines.

Image Preprocessing

A fully automated processing pipeline was applied to extract morphometric variables from structural MRI. T1-weighted image intensity inhomogeneity was corrected,⁹ followed by multiatlas skull-stripping.¹⁰ A total of 145 anatomic regions of interest (ROIs) were segmented using a multiatlas, multiwarp label fusion-based method.¹¹ Interstudy ROI harmonization was performed using the Neuroharmonize toolbox⁶ (Raymond Pomponio) (eMethods 2 in Supplement 1). White matter hyperintensities (WMHs) were segmented from fluid-attenuated inversion recovery (FLAIR) and T1-weighted images using a DL-based method.¹² A semiautomated visual quality check tool¹³ was used to manually review WMH segmentations. eTable 3 in Supplement 1 reports study imaging parameters.

Study Design

Subgroups of structural brain measures of WODCI individuals were independently examined in 4 decade-long age intervals spanning 45 to 85 years; decade intervals were used to mitigate age-related effects during clustering. The first decade spanned ages 45 years to younger than 55 years (notated 45-55 years). Participants older than 85 years were excluded due to insufficient sample availability. Within each age interval, the 145 harmonized ROI volumes were linearly corrected for continuous age, sex, and a DL-based intracranial volume measurement (DLICV)¹² to avoid biasing the clustering with

disease-unrelated neuroanatomical variations. Linear correction was performed due to the limited age range within each interval. WMH volumes were cube-root transformed due to skewness and then adjusted for the same covariates. Corrected data were standardized to *z* scores. Principal component analysis (PCA)^{14,15} was applied to anatomic ROI and WMH volumes separately for dimensionality reduction with the ultimate goal of detecting a group with low atrophy and WMH volumes called resilient brain agers (AO) (eMethods 3 and eTable 4 in Supplement 1). Using AO as a reference, heterogeneity within the remaining samples was investigated by fitting a Smile-GAN model independently for each age group. Smile-GAN was trained jointly on the 145 anatomic ROI and 8 lobar WMH volumes (eTable 5 in Supplement 1). Clustering methods¹⁶⁻¹⁸ used to quantify heterogeneity in neuroimaging are often limited by disease-irrelevant confounding variability. Smile-GAN, by learning a one-to-many mapping from the reference (AO) to the target domains (non-AO), models disease heterogeneity without being confounded by disease-unrelated factors (eg, demographics) detectable in AO (eMethods 4 in Supplement 1). PCA and Smile-GAN models trained on baseline scans were applied to available longitudinal scans within each age group.

Model Longitudinal Stability

Because clustering was performed using the model for the age at the time of scanning, we investigated whether transitioning between study-defined age decades affects clustering stability/reproducibility using individuals with longitudinal scans. We evaluated the longitudinal clustering stability for participants with scans acquired in multiple age groups, therefore clustered using independently derived models, using as reference the stability of longitudinal imaging for participants that remained within a single age group during follow-up.

Genetic Analysis

The Smile-GAN probability scores were used as phenotypes in genome-wide association studies (GWASs) using imputed genotyping data from UK Biobank. We performed multiple linear regressions controlling for continuous age, sex, DLICV, and the first 40 genetic principal components¹⁹ via Plink 2, version 2.0.0 (Christopher Chang).²⁰ Given the observed longitudinal clustering stability, GWASs were performed for the entire age range (45-85 years). Functional Mapping and Annotation²¹ was used to identify and annotate candidate single-nucleotide variants (SNVs), independent significant SNVs, (top) lead SNVs, and genomic loci (eMethods 5 in Supplement 1). We queried the top lead SNV within each locus to determine if a locus was novel—not previously associated with any clinical traits—and the candidate SNVs to explore their phenome-wide associations on GWAS Catalog.²² Additionally, we calculated SNV-based heritability estimates (h^2) using genome-wide complex trait analysis, version 1.93.2 (Yang Lab).²³ Finally, we associated the Smile-GAN probability scores with the polygenic risk score (PRS) for 2 subtypes of late-life depression (LLD1 and LLD2) developed in our previous studies.^{24,25} LLD1 was characterized by preserved brain structure, whereas LLD2 demonstrated diffuse brain atrophy.

Statistical Analysis

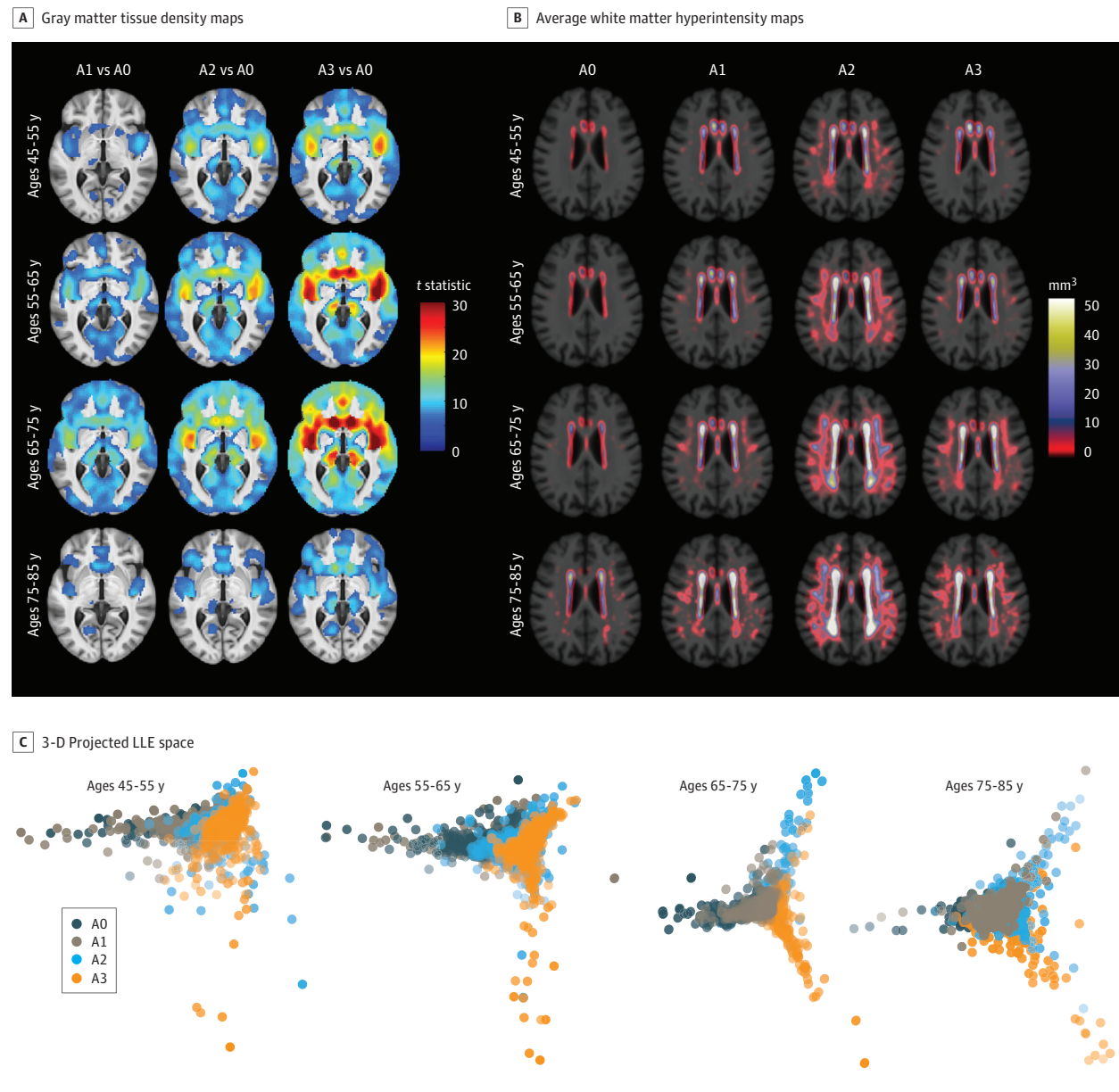
Voxel-based morphometry (VBM)^{26,27} as implemented in Statistical Parametric Mapping, version 12,²⁸ running on MATLAB, version R2017b (Mathworks Inc) was used to compare subgroups in gray matter (GM) patterns using tissue density maps (Regional Analysis of Volumes Examined in Normalized Space [RAVENS]),²⁹ considering continuous age, sex, and DLICV as covariates. Multiple-voxel testing was corrected by controlling the familywise error rate via random field theory³⁰ at 0.1%. Complementary to mass-univariate voxel-based subgroup comparisons, we also applied a manifold learning technique called locally linear embedding (LLE)^{31,32} to map high-dimensional imaging patterns into a low dimensional space that allowed visualization of multivariate data (eMethods 6 in Supplement 1).

We examined the clinical, cognitive, biomarker, and apolipoprotein E (APOE) allele associations of the subgroups in each age group separately. Linear and logistic regressions were performed for continuous (eg, Trail Making Test B) and categorical features (eg, smokers vs nonsmokers), respectively. For cognitive outcomes having overdispersed and skewed distributions (eg, MMSE), the beta-binomial distribution³³ was fitted. The regression models included subgroup labels while adjusting for continuous age, sex, and study (and education for cognitive scores). For features showing consistent trends across more than 1 age group, the data from multiple age groups were pooled together, and subgroup differences were reexamined using 1 model in the combined dataset over broader age ranges considering the study \times age interaction term. Differences across subgroup intercepts were assessed using the Wald test.³⁴ Multiple comparison corrections were conducted for the number of features by controlling the false discovery rate³⁵ at 5%.

We fit linear mixed-effects models with subject-specific random intercept to estimate the rate of change per year for atrophy, WMH, cognition, SPARE-AD (Spatial Pattern of Abnormality for Recognition of Early Alzheimer Disease)—a signature of AD-specific regional brain atrophy,³⁶ which has also been found to predict progression from normal cognition to mild cognitive impairment (MCI)³⁶—and SPARE-BA (Spatial Pattern of Atrophy for Recognition of Brain Aging)—a structural MRI-based brain age estimation.³⁷ Both SPARE models were previously validated.^{7,8,36-39} The linear mixed-effects models included subgroup indicators, time of visit, and their interaction term while adjusting for baseline age, sex, study, education, and DLICV. Rate of change subgroup comparisons were conducted using the Wald test.³⁴ The longitudinal analyses were conducted considering individuals with 4 or more longitudinal measures to reduce uncertainty in slope estimation.

Development of MCI defined by the individual participating study (eMethods 1 in Supplement 1) was used to indicate longitudinal cognitive deterioration. Survival curves for time to progression to MCI were generated using a nonparametric Kaplan-Meier estimator⁴⁰; the log-rank test⁴¹ was used to compare the curves between subgroups. All *P* values were 2-sided, and a *P* value $< .05$ was considered statistically significant. Data were analyzed from July 2021 to February 2023.

Figure 1. Structural Profile of the Brain Aging Subgroups for the 4 Age Groups



A, Significant gray matter (GM) volumetric reduction (familywise error $P < .001$) for the Smile-Generative Adversarial Network (GAN) subgroups compared with the A0 group in each age group. Voxel-based morphology comparisons between the subgroups of all age groups and the A0 group in the 45- to 55-year age groups are presented in eFigure 2 in Supplement 1. Warmer colors indicate regions with severe GM atrophy, whereas cooler colors represent lower atrophy areas. An overlay brain template in gray colors is used. B, Average white matter hyperintensity (WMH) maps computed by averaging WMH regional analysis of volumes examined in normalized space (RAVENS) maps aligned to a common

atlas space within each region of interest. Pinkish colors indicate regions with lower WMH burden, whereas whitish colors indicate high WMH burden regions. An overlay brain template in gray colors is used. C, Three-dimensional (3-D) projected locally linear embedding space derived from brain volumetric measures (eMethods 6 in Supplement 1). The data points have been colored based on the subgroup labels. This projection allows visualization of subgroups across the age groups; as a projection, the axes are not directly meaningful. LLE indicates locally linear embedding.

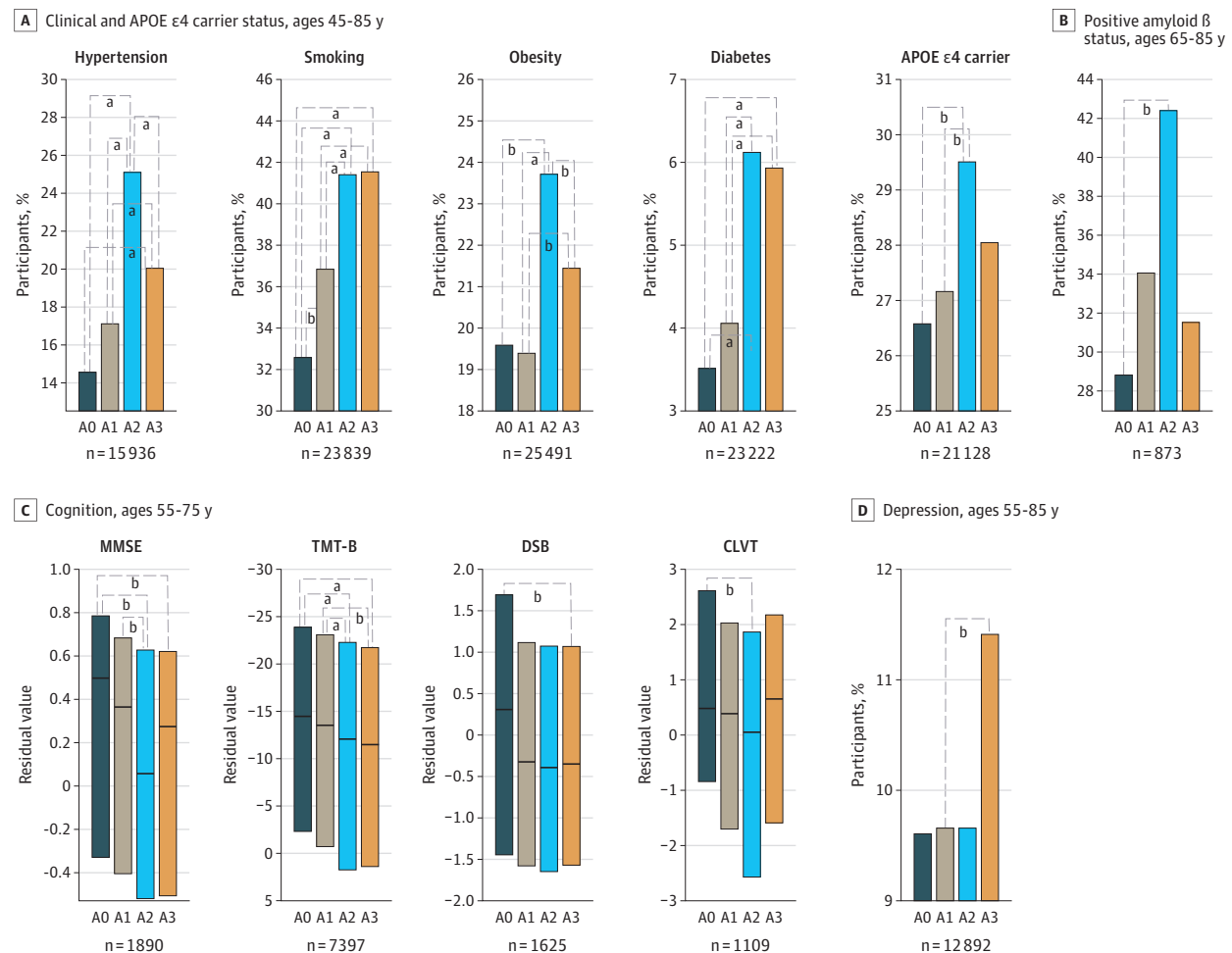
Results

Consistent Accelerated Brain Aging Patterns Across Age Groups

In this cohort study, we included 58 113 time points from 27 402 individuals (mean [SD] age, 63.0 [8.3] years; 15 146 female

[55%]; 12 256 male [45%]) WODCI. A flowchart depicting the sample selection procedure is displayed in eFigure 1 in Supplement 1. Participant demographics for baseline and longitudinal ($n = 3567$) cohorts are given in eTables 1 and 2 in Supplement 1. Participants self-identified with the following race and ethnicity categories: 313 Asian (1.1%), 838 Black (3.1%), 23 398 White (85.4%), and 2853 other (10.4%). PCA defined the A0

Figure 2. Clinical, Cognitive, Amyloid β , and Apolipoprotein E (APOE) $\epsilon 4$ Carrier Status Trends of the Brain Aging Subgroups at Baseline



The plotted features are those nonimaging features that showed consistent trends across more than one age group, presented as a summary after pooling data across age groups. The age ranges above the plots indicate the broader age groups examined. The amyloid β status (positive vs negative) was defined as described in eMethods 8 in Supplement 1. For cardiovascular risk factors and depression, the status was determined as described in eMethods 9 in Supplement 1. APOE $\epsilon 4$ carriers were considered those having 1 or 2 $\epsilon 4$ alleles. The box plots show the residuals after adjustment for continuous age, sex, and study (and education for cognitive test scores) for each subgroup (eMethods 10 in Supplement 1). Higher Mini-Mental State Examination (MMSE), Digit Span Backward (DSB), and California Verbal Learning Test (CVLT) scores indicate

better cognition, whereas lower Trail Making Test B (TMT-B) scores indicates better cognition; TMT scores are presented with an inverted scale, therefore, poorer cognitive performance is in the same direction across the 4 graphs. The horizontal line shows the median value. The bar plots show the percentage of participants with various risk factors for each subgroup. N indicates the sample size for the graph. False discovery rate correction for multiple comparisons with a P value threshold of .05 was applied. The complete list of features found consistent across more than 1 decade is given in eTable 10 in Supplement 1.

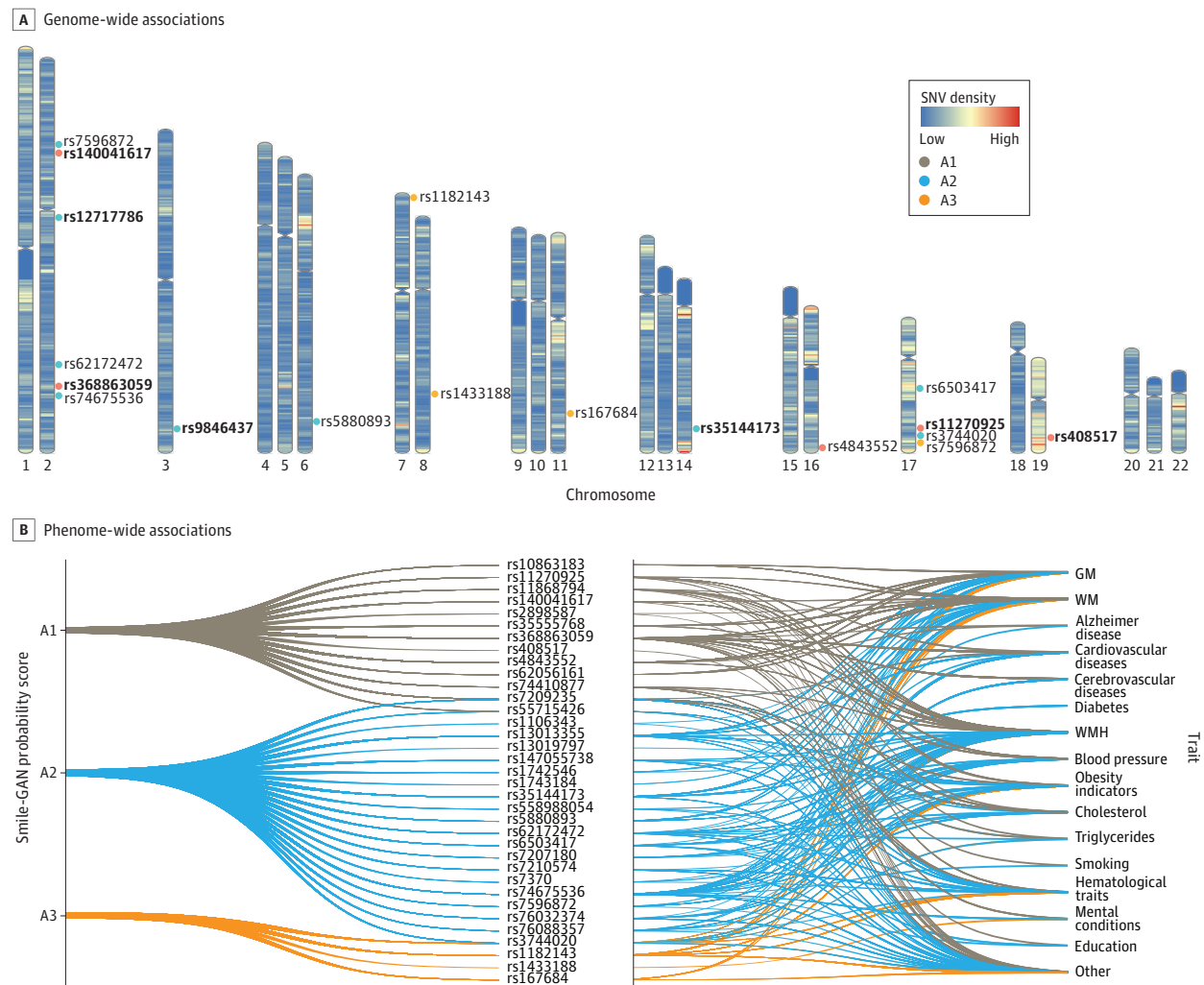
^a $P < .001$.

^b $P < .05$.

resilient group as participants with the lowest atrophy and WMH volume within each age group. Referenced to A0, Smile-GAN showed optimal stability for 3 clusters ($k = 3$), measured by the Adjusted Rand Index^{42,43} (eTable 6 in Supplement 1). Two types of phenotypes from this clustering scheme were used for subsequent analyses. The Smile-GAN subgroup probability was the direct model output, representing a continuous variable for each of the 3 clusters for each participant, with the sum of these 3 probabilities equaling 1; the Smile-GAN subgroup was decided by taking the highest probability (dominant subgroup). Although derived independently by age decade, the Smile-GAN subgroups, A1, A2, and A3, showed consistent differences in atrophy and WMH load

compared with A0 (Figure 1A). A1 showed mild, predominantly peri-Sylvian atrophy. A2 displayed greater peri-Sylvian atrophy accompanied by atrophy in orbitofrontal and other prefrontal regions. A3 had diffuse atrophy across the brain, including the medial frontal regions and thalamus. WMH burden was higher in A2 than in the other subgroups (Figure 1B). Among A1, A2, and A3, A1 had the least atrophy and was the largest subgroup, therefore, it may be considered typical aging. In comparison, A2 (highest lesions) and A3 (most severe atrophy) are considered accelerated aging subgroups. VBM within the 75- to 85-year age group showed less prominent between-subgroup differences due to relatively more advanced atrophy in the 75- to 85-year age group in A0

Figure 3. Genetic Analyses of the Smile-Generative Adversarial Network (GAN) Probability Scores (A1, A2, and A3)



A, GWAS identified genomic loci (represented by the top lead SNP) associated with the Smile-GAN probability scores (A1, A2, and A3). The genome-wide P value threshold (5×10^{-8}) was used in all genome-wide association studies (GWASs). We denote a locus as novel (the lead single-nucleotide variant [SNV] represented by bold font) if it was not associated with any clinical traits in GWAS Catalog.²² The reference genome is Genome Reference Consortium Human Build 37 (GRCh37). The ideogram plot represents all autosomal chromosomes (1-22). Manhattan and quantile-quantile plots are presented in eFigures 6 and 7 in Supplement 1. An exemplary genomic locus associated with the A2 probability score is shown in eFigure 8 and eTable 13 in Supplement 1.

B, Phenome-wide associations from the GWAS Catalog. Independent significant

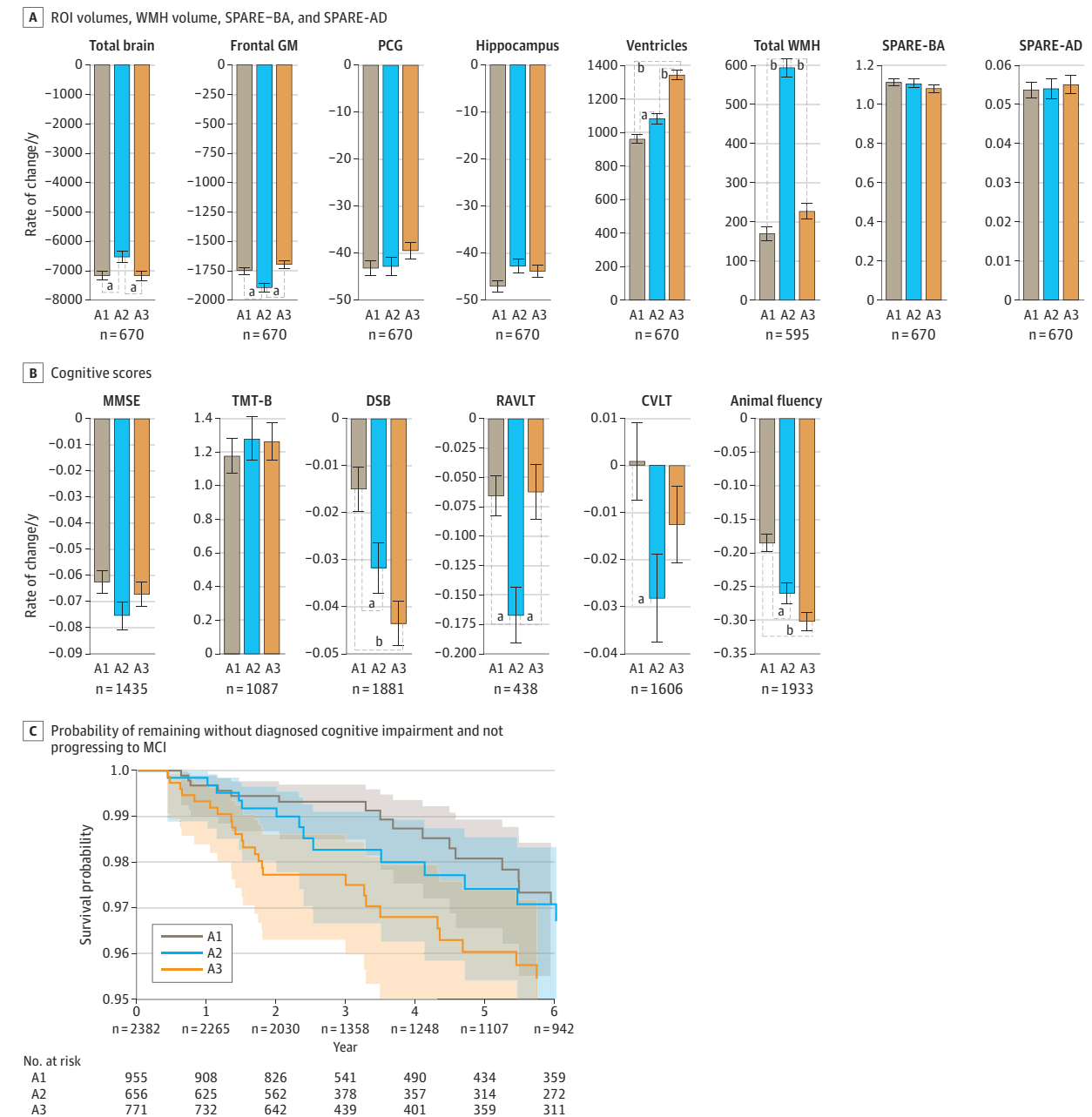
SNVs inside each locus were associated with many clinical traits, which were further classified into high-level groups, including gray matter (GM) measures (eg, [sub]cortical volume, cortical thickness, and surface area), white matter (WM) measures (eg, whole-brain-restricted isotropic diffusion and whole-brain-free water diffusion), cardiovascular diseases (eg, coronary artery disease and myocardial infarction), cerebrovascular diseases (eg, nonlobar intracerebral hemorrhage and stroke), hematological traits (eg, platelet, eosinophil, and white blood cell counts), mental conditions (eg, risk-taking behavior and suicide attempts), etc. We also found individual traits such as Alzheimer disease, white matter hyperintensities (WMHs), cardiovascular risk factors, education, and others.

compared with younger A0 groups and more structural variability in this age group (Figure 1A; and eFigure 2 in Supplement 1). The average brain age difference between the youngest- and oldest-appearing brains (A0 vs A3) was approximately 10 years and relatively consistent across age groups (eFigure 3 in Supplement 1).

We found that longitudinal scans within 1 age interval showed approximately 85% consistency of cluster assignment. We observed approximately 80% longitudinal stability of clustering assignments in participants who aged into the next interval within a follow-up of 3 years or less,

even though entirely independent clustering models were applied to scans at the different age intervals (eg, participants classified as A2 using the 55-65 years model were mostly classified as A2 on follow-up scans using the 65-75 years model). Furthermore, eTables 7 and 8 in Supplement 1 display the mean Smile-GAN probability shifts between 2 consecutive scans within the same age group and across different age groups, respectively. Our findings indicate that the magnitude of probability changes across decades was comparable with those observed within the same decade.

Figure 4. Longitudinal Outcomes



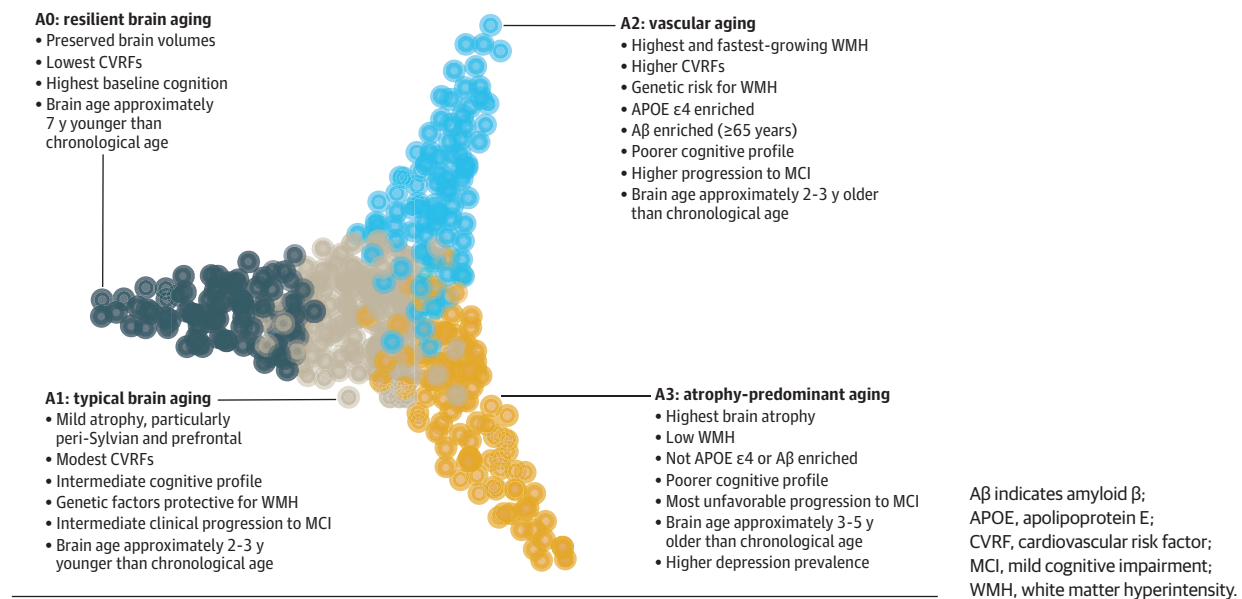
Rate of change per year for region of interest (ROI) and white matter hyperintensity (WMH) volumes (units: mm³), Spatial Pattern of Atrophy for Recognition of Brain Aging (SPARE-BA), Spatial Pattern of Abnormality for Recognition of Early Alzheimer Disease (SPARE-AD; unitless) (A) and cognitive scores calculated using linear mixed-effects models with subject-specific random intercept for the Smile-Generative Adversarial Network (GAN) brain aging subgroups (B). The models included subgroup indicators, time of visit, and their interaction term while adjusting for baseline age, sex, study, education, and deep learning-based intracranial volume measurement (DLICV). Subgroup comparisons of rates of change were conducted using the Wald test. N indicates the number of individuals having 4 or more longitudinal measures for the plotted feature. False discovery rate correction for multiple comparisons was used with a *P* value threshold of .05. The *P* values are given in eTable 14 in Supplement 1. The rate of change for ventricles, SPARE scores, total WMH, and Trail Making Test B (TMT-B) are presented with an inverted scale, therefore, faster brain aging (reflected by either more rapid atrophy, lesions accumulation,

or cognitive decline) is in the same direction across graphs. C, Kaplan-Meier survival curves show the probability of remaining participants without diagnosed cognitive impairment (WODCI) and not progressing to mild cognitive impairment (MCI) for individuals with a baseline age within the 65- to 75-year range. N indicates the number of individuals followed up for each time interval. Log-rank test was used to compare the survival curves of the Smile-GAN subgroups. The only significant difference is between A1 and A3 curves (*P* value = .01). Longitudinal results for A0 are not shown because the A0 group was derived using a different methodology from the Smile-GAN subgroups. Additionally, the sample size for longitudinal A0 was small, and thus, the results were not robust. CVLT indicates California Verbal Learning Test; DSB, Digit Span Backward; GM, gray matter; MMSE, Mini-Mental State Examination; PCG, Posterior Cingulate Gyrus; RAVLT, Rey Auditory Verbal Learning Test.

^a *P* < .001.

^b *P* < .05.

Figure 5. Schematic Summary of Key Features of the Brain Aging Subgroups



Branched Continuum Across Resilient, Typical, and Accelerated Aging

Although VBM suggested a primary difference in severity across subgroups, examination of differences in location and severity of atrophy identified unique volumetric fingerprints across subgroups. Figure 1C shows the 3-dimensional projected LLE space derived from brain volumetric measures, revealing worse atrophy in A1 compared with A0, followed by diverging branches for A2 and A3, especially after age 65 years. These axes echo the variability of distances between regional measures seen in radial plots (eMethods 7 and eFigure 4 in Supplement 1). WMH volumes were not included in LLE analyses; the 2-axes divergence exclusively reflects atrophy subgroups and not the distinct difference in WMH burden.

Clinical, Cognitive, Biomarker and APOE ϵ 4 Genotype Features

We examined between-subgroup differences in clinical and cognitive features, A β , and APOE ϵ 4 carrier status for each age group separately (eTable 9 in Supplement 1). eFigure 5 in Supplement 1 shows the complete list of features examined and their availability. Features that showed consistent trends across more than 1 age group are summarized in Figure 2 after reanalyzing pooling data. Consistent with the known association of cardiovascular disease (CVD) and WMH, we found that A2 had the highest proportion of participants with cardiovascular risk factors (CVRFs), including hypertension and obesity. A2 and A3 had similarly higher proportions of smokers and individuals with diabetes than A0 and A1.

Although A2 did not show the most severe atrophy, it had the highest prevalence of APOE ϵ 4 carriers and, after age 65 years, the most elevated proportion of cerebral A β positivity (A β +). However, trends toward a higher

prevalence of APOE ϵ 4 carriers and higher A β + prevalence in A2 vs A3 were not statistically significant (eTable 10 in Supplement 1). Regarding A β measures, the only statistically significant difference was the higher prevalence of A β + in A2 compared with A0. These findings suggest that none of the Smile-GAN subgroups were specifically an early AD-related group, but the A2 subgroup had a higher prevalence of AD pathologic change.

Although participants were selected as not having been diagnosed with cognitive impairment, the A2 and A3 accelerated aging subgroups showed poorer cognitive test performance compared with the A0 and A1 subgroups for ages 55 to 75 years. Despite different structural features, A2 and A3 did not differ significantly in cognitive performance across domains. Thus, poorer cognitive performance in A2 and A3 appears to reflect additive effects of atrophy and WMH. Additionally, A3 had the highest proportion of individuals experiencing depression after age 55 years.

Genome-Wide Associations of the Smile-GAN Probability Scores

The Smile-GAN probability scores (A1, A2, and A3) were associated with 5, 9, and 4 genomic loci, respectively. Several loci were previously identified, whereas others were novel (Figure 3A and eTable 11 in Supplement 1). An exemplary genomic locus associated with the A2 probability score is shown in eFigure 8 and eTable 13 in Supplement 1. These previously identified loci were associated with various clinical traits, including imaging-derived phenotypes from white matter microstructure (A1-3),⁴⁴ gray matter atrophy (A1-3),⁴⁵ WMH (A1-3),⁴⁶ CVRFs (A1-2),⁴⁷ CVD (A1-2),⁴⁸ and AD (A1-2)⁴⁹ (Figure 3B). The GWAS Catalog query is detailed in the eFigure in Supplement 2.

Several SNVs exerted pleiotropic effects on more than 1 phenotype/probability with opposite directions of

the association effects. For example, A1 (mean [SD] $B = -0.07$ [0.01]; P value = 2.31×10^{-9} and mean [SD] $B = -0.09$ [0.02]; P value = 4.09×10^{-8}) and A2 (mean [SD] $B = 0.1$ [0.01]; P value = 1.73×10^{-15} and mean [SD] $B = 0.13$ [0.02]; P value = 1.04×10^{-15}) were associated with the 2 novel independent variants (rs7209235 and rs55715426 at cytogenetic region:17q25.1), whose mapped genes *GALK1* and *H3-3B* were associated with several CVD biomarkers, including cholesterol⁵⁰ and apolipoprotein B.⁵¹ Therefore, these variants may be protective against CVD for A1 but may serve as risk variants for A2. Furthermore, A1 (mean [SD] $B = 0.1$ [0.02]; P value = 6.49×10^{-9}) and A2 (mean [SD] $B = -0.09$ [0.02]; P value = 4.05×10^{-7}) were both associated with the candidate SNV rs72932727 (cytogenetic position:2q33.2) previously associated with the AD PRS.⁴⁹ Because A2 had the highest prevalence of APOE $\epsilon 4$ carriers and participants who were $A\beta+$, opposite to A1, rs72932727 may play a protective role against AD for A1 and may be a risk factor for A2.

Finally, variants in A3 were associated with regional atrophy (rs167684: mean [SD] $B = 0.08$ [0.01]; P value = 7.22×10^{-12}) and white matter integrity measures (rs1636250: mean [SD] $B = 0.06$ [0.01]; P value = 4.90×10^{-7}). A3 was significantly associated with both PRS-LLD1 and LLD2 with opposite direction association effects (LLD1: mean [SD] $B = -0.05$ [0.01]; P value < .001, LLD2: mean [SD] $B = 0.05$ [0.01]; P value = .001). A1 was associated with the PRS-LLD1 (mean [SD] $B = 0.04$ [0.02]; P value = .007), with LLD1 characterized by preserved brain volume (eTable 12 in Supplement 1). Moreover, the imaging-derived phenotypes showed highly significant SNV-based heritability estimates (A1: $h^2 = 0.44$ [0.04], A2: $h^2 = 0.55$ [0.04], A3: $h^2 = 0.45$ [0.04]; all P values < 10^{-4}).

Longitudinal Outcomes

Across individuals with 4 or more longitudinal MRI scans ($n = 670$; mean [SD] follow-up, 8.0 [4.7] years; baseline mean [SD] age, 69.2 [8.9] years), we observed small differences between subgroups in longitudinal atrophy (Figure 4 and eTable 14 in Supplement 1). Progression of WMH ($n = 595$; mean [SD] follow-up, 8.1 [4.9] years; baseline mean [SD] age, 69.3 [8.9]) was significantly faster in A2. A2 and A3 subgroups showed the greatest longitudinal cognitive decline (number of individuals with longitudinal cognitive scores was 438 to 1933, mean [SD] longitudinal cognitive testing was over 5.0 [2.6] years to 8.0 [4.7] years across tests, and mean [SD] baseline age was over 69.4 [6.5] years to 70.7 [8.4] years across tests) in agreement with the faster progression from cognitively unimpaired to MCI (Figure 4C), emphasizing the long-term implications of the baseline MRI subgroups.

Discussion

Genetics, lifestyle, CVRFs, and neuropathologies modify brain aging heterogeneously across individuals even before cognitive symptoms are expressed. We applied advanced DL

methods to a large, diverse, harmonized multicohort sample to find characteristic neuroanatomical subgroups of brain variation. Consistent subgroups of brain aging emerged in each of the decade-long intervals between 45 and 85 years: A1, or typical aging subgroup with low atrophy and WMH load, and 2 accelerated aging subgroups, A2 and A3. Thus, we observed heterogeneity of brain aging in the WODCI population with stable patterns across decades. These subgroups were detectable from midlife and had associations with cardiometabolic and genetic risk factors and cognition (Figure 5).

One of our primary findings was the emergence of 2 accelerated brain aging trajectories, best visualized from the manifold algorithm, which were particularly distinct in individuals 65 years and older. A2 was associated with hypertension, WMH, and vascular disease-associated genetic risk factors, evidenced by the GWAS (Figure 3A), and opposite from the protective effect in A1. This subgroup was also mildly enriched for $A\beta+$ (ages ≥ 65 years) and AD-related genetic risk factors, including APOE $\epsilon 4$. A3 showed widespread GM atrophy and moderate presence of CVRFs. Thus, A2 and A3 may have different brain reserve,⁵² affecting susceptibility to future pathology.

Despite differences in patterns of atrophy, A2 and A3 had comparable poorer cognitive functions than A0. Thus, atrophy and WMH seem to act additively to cause cognitive decline. This may account for lower atrophy in A2 vs A3; further atrophy may predispose to conversion to MCI, resulting in exclusion from this WODCI cohort. Although we did not define underlying pathology related to neuroimaging findings, such an effect is comparable with prior studies showing that the combined involvement of neurodegenerative and vascular pathology is more pronounced in the earliest stages of cognitive impairment.^{53,54} All subgroups had low SPARE-AD scores, indicating no significant AD-related neurodegeneration. Overall, $A\beta+$ individuals represented a minority and were relatively evenly distributed across subgroups, suggesting that factors influencing structural brain aging in this WODCI population may be largely independent of AD before the emergence of symptoms. A3, on the other hand, was not uniquely enriched in a particular studied cardiovascular risk factor; it had the highest prevalence of depression, and the A3 probability score was associated with depression-related PRS. Further investigation of the association of A3 with other risk factors is warranted to understand this group better.

Strengths and Limitations

This study has several strengths, including the large, diverse, multisite sample covering a wide age range and the use of advanced harmonization and DL methods. Additionally, identifying multiple SNVs associated with WMH and brain atrophy is consistent with the neuroimaging profile of the subgroups. However, this study also has limitations. First, the heterogeneity in sampling strategies and data acquisition of each contributing study might impede generalization. Second, there is low availability of amyloid data and insufficient availability of tau measures and biomarkers related to

non-AD neurodegeneration. Third, the lack of long-term follow-up prevents the derivation of robust conclusions regarding the clinical progression and transition to MCI. Fourth, regarding sample composition, there is a ceiling effect as people with more severe findings are more likely to be classified as cognitively impaired and thus be excluded from the sample. Fifth, although we have observed certain morphologic and correlation similarities of subgroups across decades, the equivalence of the subgroups across decades cannot be proved because different models were used in each decade, and there was not substantial follow-up across decades.

Conclusions

In this multicohort study, consistent and reproducible neuroimaging subgroups defined by regional atrophy and WMH burden were identified across individuals aged 45 to 85 years without diagnosed cognitive impairment. Two axes of accelerated aging emerged, one showing elevated CVRFs and enrichment of cerebral A β and the other with more diffuse and severe atrophy. These subgroups likely reflect differential susceptibility to AD and other neurodegenerative diseases, cognitive decline, and clinical progression.

ARTICLE INFORMATION

Accepted for Publication: November 29, 2023.

Published Online: February 14, 2024.

doi:10.1001/jamapsychiatry.2023.5599

Author Affiliations: Centre for Biomedical Image Computing and Analytics, University of Pennsylvania, Philadelphia (Skampardoni, Nasrallah, Abdulkadir, Wen, Melhem, Mamourian, Erus, Doshi, Singh, Yang, Cui, Hwang, Pomponio, Srinivasan, Govindarajan, Parmpi, Shinohara, Fan, Habes, Shou, Davatzikos); School of Electrical and Computer Engineering, National Technical University of Athens, Greece (Skampardoni, Nikita); Department of Radiology, University of Pennsylvania, Philadelphia (Nasrallah, Bryan); Laboratory for Research in Neuroimaging, Department of Clinical Neurosciences, Lausanne University Hospital and University of Lausanne, Lausanne, Switzerland (Abdulkadir); Laboratory of AI and Biomedical Science, Stevens Neuroimaging and Informatics Institute, Keck School of Medicine of USC, University of Southern California, Los Angeles (Wen, Ren); Penn Statistics in Imaging and Visualization Center, Department of Biostatistics, Epidemiology, & Informatics, University of Pennsylvania, Philadelphia (Shinohara, Shou); Department of Psychiatry and Psychotherapy, University Medicine Greifswald, Germany (Wittfeld, Grabe, Frenzel); German Centre for Neurodegenerative Diseases, Site Greifswald, Greifswald, Germany (Wittfeld, Grabe); Institute of Diagnostic Radiology and Neuroradiology, University Medicine Greifswald, Greifswald, Germany (Bülow); Department of Radiology and Biomedical Imaging, University of California, San Francisco (Tosun); Laboratory of Behavioral Neuroscience, National Institute on Aging, National Institutes of Health, Baltimore, Maryland (Bilgel, An, Resnick); Department of Radiology, Washington University School of Medicine, St Louis, Missouri (Marcus, LaMontagne); Cardiovascular Health Research Unit, University of Washington, Seattle (Heckbert, Austin); Department of Epidemiology, University of Washington, Seattle (Heckbert, Austin); Neuroepidemiology Section, Intramural Research Program, National Institute on Aging, Bethesda, Maryland (Launer); Department of Radiology and Institute of Informatics, Washington University in St Louis, St Louis, Missouri (Sotiras); Sticht Centre for Healthy Aging and Alzheimer's Prevention, Wake Forest School of Medicine, Winston-Salem, North Carolina (Espeland); Department of Biostatistics and Data Science, Wake Forest School of Medicine, Winston-Salem, North Carolina (Espeland); Florey Institute of

Neuroscience and Mental Health, The University of Melbourne, Parkville, Victoria, Australia (Masters, Maruff); CSIRO Health and Biosecurity, Australian e-Health Research Centre CSIRO, Brisbane, Queensland, Australia (Fripp); Wisconsin Alzheimer's Institute, University of Wisconsin School of Medicine and Public Health, Madison (Johnson); Knight Alzheimer Disease Research Centre, Washington University in St Louis, St Louis, Missouri (Morris); Department of Neurology, Johns Hopkins University School of Medicine, Baltimore, Maryland (Albert); Departments of Neurology, Psychiatry and Epidemiology and Biostatistics, University of California San Francisco, San Francisco (Yaffe); Institute for Community Medicine, University Medicine Greifswald, Greifswald, Germany (Völzke); Translational Gerontology Branch, National Institute on Aging, National Institutes of Health, Baltimore, Maryland (Ferrucci); Mallinckrodt Institute of Radiology, Washington University School of Medicine in St Louis, St Louis, Missouri (Benzinger); Department of Neurology, University of California, Irvine (Ezzati); Neuroimage Analytics Laboratory and the Biggs Institute Neuroimaging Core, Glenn Biggs Institute for Alzheimer's and Neurodegenerative Diseases, University of Texas Health Science Center San Antonio, San Antonio (Habes); Department of Neurology, University of Pennsylvania, Philadelphia (Wolk).

Author Contributions: Dr Davatzikos had full access to all of the data in the study and takes responsibility for the integrity of the data and the accuracy of the data analysis. Ms Skampardoni and Drs Nasrallah and Abdulkadir equally contributed to this work.

Concept and design: Skampardoni, Nasrallah, Abdulkadir, Wen, Buelow, Marcus, Masters, Morris, Ferrucci, Davatzikos.

Acquisition, analysis, or interpretation of data: Skampardoni, Nasrallah, Abdulkadir, Wen, Melhem, Mamourian, Erus, Doshi, Singh, Yang, Cui, Hwang, Ren, Pomponio, Srinivasan, Tirumalai Govindarajan, Parmpi, Wittfeld, Grabe, Buelow, Frenzel, Tosun, Bilgel, An, LaMontagne, Heckbert, Austin, Launer, Sotiras, Espeland, Maruff, Fripp, Johnson, Morris, Albert, Bryan, Yaffe, Voelzke, Benzinger, Ezzati, Shinohara, Fan, Resnick, Habes, Wolk, Shou, Nikita, Davatzikos.

Drafting of the manuscript: Skampardoni, Nasrallah, Abdulkadir, Wen, Melhem, Singh, Tirumalai Govindarajan, Maruff.

Critical review of the manuscript for important intellectual content: Skampardoni, Nasrallah, Abdulkadir, Wen, Mamourian, Erus, Doshi, Yang, Cui, Hwang, Ren, Pomponio, Srinivasan,

Tirumalai Govindarajan, Parmpi, Wittfeld, Grabe, Buelow, Frenzel, Tosun, Bilgel, An, Marcus, LaMontagne, Heckbert, Austin, Launer, Sotiras, Espeland, Masters, Fripp, Johnson, Morris, Albert, Bryan, Yaffe, Voelzke, Ferrucci, Benzinger, Ezzati, Shinohara, Fan, Resnick, Habes, Wolk, Shou, Nikita, Davatzikos.

Statistical analysis: Skampardoni, Nasrallah, Abdulkadir, Wen, Erus, Doshi, Singh, Ren, Tirumalai Govindarajan, Tosun, Bilgel, An, Morris, Shinohara, Shou.

Obtained funding: Espeland, Maruff, Johnson, Albert, Bryan, Voelzke, Benzinger, Resnick, Wolk, Davatzikos.

Administrative, technical, or material support: Nasrallah, Melhem, Mamourian, Erus, Singh, Yang, Hwang, Pomponio, Tirumalai Govindarajan, Parmpi, Grabe, Buelow, Frenzel, Tosun, Marcus, LaMontagne, Espeland, Fripp, Bryan, Benzinger, Ezzati, Fan, Davatzikos.

Supervision: Nasrallah, Abdulkadir, Tirumalai Govindarajan, Buelow, Masters, Maruff, Morris, Ferrucci, Benzinger, Davatzikos.

Conflict of Interest Disclosures: Dr Nasrallah reported receiving grants from the National Institutes of Health during the conduct of the study. Dr Abdulkadir reported receiving grants from Swiss National Science Foundation during the conduct of the study. Dr Grabe reported receiving grants from Siemens Healthineers, Federal State of Mecklenburg-West Pomerania, and Fresenius Medical Care and personal fees from Janssen Cilag, Neuraxpharm, and Servier outside the submitted work. Dr Marcus reported receiving equity in Flywheel outside the submitted work. Dr Heckbert reported receiving grants from the National Institutes of Health during the conduct of the study. Dr Austin reported receiving grants from the National Institutes of Health outside the submitted work. Dr Sotiras reported receiving personal fees from BrightFocus for serving as a grant reviewer and stock from TheraPanacea outside the submitted work. Dr Espeland reported receiving grants from the National Institutes of Health and Alzheimer's Association and personal fees from Nestle outside the submitted work. Dr Maruff reported being a full-time employee of Cogstate Ltd during the conduct of the study. Dr Johnson reported receiving advisory board fees from Alzpath and Enigma outside the submitted work. Dr Morris reported receiving grants from the National Institute of Health during the conduct of the study. Dr Bryan reported receiving grants from the National Institutes of Health during the conduct of the study. Dr Benzinger reported receiving grants from the National Institutes of Health and Siemens

and advisory board fees from Eisai, Lilly, and Biogen outside the submitted work. Dr Ezzati reported receiving grants from the National Institutes of Health, Alzheimer's Association, and Cure Alzheimer's Fund and personal fees from Corium, PCORI Horizon, and from Mist Research outside the submitted work. Dr Shinohara reported receiving grants from the National Institutes of Health during the conduct of the study. Dr Fan reported receiving personal fees from Hura Imaging outside the submitted work. Dr Wolk reported receiving grants from Biogen and personal fees from Eli Lilly, Functional Neuromodulation, and Qynapse outside the submitted work. Dr Davatzikos reported receiving grants from the National Institutes of Health during the conduct of the study. No other disclosures were reported.

Funding/Support: The Imaging-Based Coordinate System for Aging and Neurodegenerative Diseases (iSTAGING) consortium was funded by grant RF1 AG054409 from the National Institute on Aging. The Baltimore Longitudinal Study of Aging neuroimaging study is funded by the Intramural Research Program, National Institute on Aging, National Institutes of Health, and grant HHSN271201600059C from the National Institutes of Health. The Biomarkers for Older Controls at Risk for Dementia (BIOCARD) study is in part supported by a National Institutes of Health grant U19-AG033655. Other supporting funds include grants U01 AG068057, U24AG074855, S10 ODO23495, P50 AG00561, P30 NS09857781, P01 AG026276, P01 AG003991, R01 AG043434, U11 TRO00448, and R01 EBO09352 from the National Institutes of Health. AV-45 doses were provided by Avid Radiopharmaceuticals, a wholly owned subsidiary of Eli Lilly. The Alzheimer's Disease Neuroimaging Initiative is funded by the National Institute on Aging, the National Institute of Biomedical Imaging and Bioengineering, and through generous contributions from the following: AbbVie, Alzheimer's Association, Alzheimer's Drug Discovery Foundation, Araclon Biotech, BioClinica, Biogen, Bristol Myers Squibb, CereSpir, Cogstate, Eisai, Elan Pharmaceuticals, Eli Lilly and Company, EuroImmun, F. Hoffmann-La Roche and Genentech, Fujirebio, GE Healthcare, IXICO, Janssen Alzheimer Immunotherapy Research & Development, Johnson & Johnson Pharmaceutical Research & Development, Lumosity, Lundbeck, Merck & Co, Meso Scale Diagnostics, NeuroRx Research, Neurotrack Technologies, Novartis Pharmaceuticals Corp, Pfizer, Piramal Imaging, Servier, Takeda Pharmaceutical Company, and Transition Therapeutics. The Canadian Institutes of Health Research provides funds to support the Alzheimer's Disease Neuroimaging Initiative clinical sites in Canada. Dr Habes was supported by grant 1R01AG080821 from the National Institutes of Health. Study of Health in Pomerania (SHIP) is part of the Community Medicine Research Network of the University Medicine Greifswald, supported by the German Federal State of Mecklenburg-West Pomerania.

Role of the Funder/Sponsor: The funders had no role in the design and conduct of the study; collection, management, analysis, and interpretation of the data; preparation, review, or approval of the manuscript; and decision to submit the manuscript for publication.

Data Sharing Statement: See Supplement 3.

Additional Information: The data used in this study were part of the following 5 consortia: iSTAGING consortium, Preclinical AD consortium, Alzheimer's Disease Neuroimaging Initiative, Baltimore Longitudinal Study of Aging, and Coronary Artery Risk Development in Young Adults Study.

REFERENCES

1. Trofimova O, Loued-Khenissi L, DiDomenicantonio G, et al. Brain tissue properties link cardiovascular risk factors, mood, and cognitive performance in the CoLausPsyColaus epidemiological cohort. *Neurobiol Aging*. 2021;102:50-63. doi:10.1016/j.neurobiolaging.2021.02.002
2. Dubois B, Hampel H, Feldman HH, et al; Proceedings of the Meeting of the International Working Group (IWG) and the American Alzheimer's Association on "The Preclinical State of AD"; July 23, 2015; Washington DC, USA. Preclinical Alzheimer disease: definition, natural history, and diagnostic criteria. *Alzheimers Dement*. 2016;12(3):292-323. doi:10.1016/j.jalz.2016.02.002
3. Wan SH, Vogel MW, Chen HH. Preclinical diastolic dysfunction. *J Am Coll Cardiol*. 2014;63(5):407-416. doi:10.1016/j.jacc.2013.10.063
4. Goodfellow I, Pouget-Abadie J, Mirza M, et al. Generative adversarial nets. Accessed September 25, 2023. https://proceedings.neurips.cc/paper_files/paper/2014/file/5ca3e9b122f61f8f06494c97b1afcc3-Paper.pdf
5. Yang Z, Nasrallah IM, Shou H, et al; iSTAGING Consortium; Baltimore Longitudinal Study of Aging (BLSA); Alzheimer's Disease Neuroimaging Initiative (ADNI). A deep learning framework identifies dimensional representations of Alzheimer disease from brain structure. *Nat Commun*. 2021;12(1):7065. doi:10.1038/s41467-021-26703-z
6. Pomponio R, Erus G, Habes M, et al. Harmonization of large MRI datasets for the analysis of brain imaging patterns throughout the lifespan. *Neuroimage*. 2020;208:116450. doi:10.1016/j.neuroimage.2019.116450
7. Habes M, Pomponio R, Shou H, et al; iSTAGING consortium, the Preclinical AD consortium, the ADNI, and the CARDIA studies. The brain chart of aging: machine-learning analytics reveals links between brain aging, white matter disease, amyloid burden, and cognition in the iSTAGING consortium of 10 216 harmonized MR scans. *Alzheimers Dement*. 2021;17(1):89-102. doi:10.1002/alz.12178
8. Hwang G, Abdulkadir A, Erus G, et al; iSTAGING Consortium; ADNI. Disentangling Alzheimer disease neurodegeneration from typical brain aging using MRI and machine learning. *Brain Commun*. 2022;4(3):fca117. doi:10.1093/braincomms/fca117
9. Tustison NJ, Avants BB, Cook PA, et al. N4ITK: improved N3 bias correction. *IEEE Trans Med Imaging*. 2010;29(6):1310-1320. doi:10.1109/TMI.2010.2046908
10. Doshi J, Erus G, Ou Y, Gaonkar B, Davatzikos C. Multiatlas skull-stripping. *Acad Radiol*. 2013;20(12):1566-1576. doi:10.1016/j.acra.2013.09.010
11. Doshi J, Erus G, Ou Y, et al; Alzheimer's Neuroimaging Initiative. MUSE: multiatlas region segmentation utilizing ensembles of registration algorithms and parameters, and locally optimal atlas selection. *Neuroimage*. 2016;127:186-195. doi:10.1016/j.neuroimage.2015.11.073
12. Doshi J, Erus G, Habes M, Davatzikos C. DeepMRSeg: a convolutional deep neural network for anatomy and abnormality segmentation on MR images. <http://arxiv.org/abs/1907.02110>.
13. Github. CBICA/MRISnapshot. Accessed November 21, 2022. <https://github.com/CBICA/MRISnapshot>
14. Jolliffe IT. *Principal Component Analysis*. Springer-Verlag; 1986.
15. Jackson JE. *A User's Guide to Principal Components*. Wiley-Interscience; 2003.
16. Noh Y, Jeon S, Lee JM, et al. Anatomical heterogeneity of Alzheimer disease: based on cortical thickness on MRIs. *Neurology*. 2014;83(21):1936-1944. doi:10.1212/WNL.0000000000001003
17. Poulakis K, Pereira JB, Mecocci P, et al. Heterogeneous patterns of brain atrophy in Alzheimer disease. *Neurobiol Aging*. 2018;65:98-108. doi:10.1016/j.neurobiolaging.2018.01.009
18. Ten Kate M, Dicks E, Visser PJ, et al; Alzheimer's Disease Neuroimaging Initiative. Atrophy subtypes in prodromal Alzheimer disease are associated with cognitive decline. *Brain*. 2018;141(12):3443-3456. doi:10.1093/brain/awy264
19. Wen J, Nasrallah IM, Abdulkadir A, et al. Genomic loci influence patterns of structural covariance in the human brain. *Proc Natl Acad Sci U S A*. 2023;120(52):e2300842120. doi:10.1073/pnas.2300842120
20. Purcell S, Neale B, Todd-Brown K, et al. PLINK: a tool set for whole-genome association and population-based linkage analyses. *Am J Hum Genet*. 2007;81(3):559-575. doi:10.1086/519795
21. Watanabe K, Taskesen E, van Bochoven A, Posthuma D. Functional mapping and annotation of genetic associations with FUMA. *Nat Commun*. 2017;8(1):1826. doi:10.1038/s41467-017-01261-5
22. Buniello A, MacArthur JAL, Cerezo M, et al. The NHGRI-EBI GWAS Catalog of published genome-wide association studies, targeted arrays and summary statistics 2019. *Nucleic Acids Res*. 2019;47(D1):D1005-D1012. doi:10.1093/nar/gky1120
23. Yang J, Lee SH, Goddard ME, Visscher PM. GCTA: a tool for genome-wide complex trait analysis. *Am J Hum Genet*. 2011;88(1):76-82. doi:10.1016/j.ajhg.2010.11.011
24. Wen J, Fu CHY, Tosun D, et al; iSTAGING Consortium, ADNI, BIOCARD, and BLSA. Characterizing heterogeneity in neuroimaging, cognition, clinical symptoms, and genetics among patients with late-life depression. *JAMA Psychiatry*. 2022;79(5):464-474. doi:10.1001/jamapsychiatry.2022.0020
25. Wen J, Skampardonio I, Tian YE, et al. Neuroimaging-AI endophenotypes of brain diseases in the general population: toward a dimensional system of vulnerability. *medRxiv*. Preprint posted online August 24, 2023. doi:10.1101/2023.08.16.23294179
26. Ashburner J, Friston KJ. Voxel-based morphometry—the methods. *Neuroimage*. 2000;11(6 Pt 1):805-821. doi:10.1006/nimg.2000.0582
27. Wright IC, McGuire PK, Poline JB, et al. A voxel-based method for the statistical analysis of gray and white matter density applied to schizophrenia. *Neuroimage*. 1995;2(4):244-252. doi:10.1006/nimg.1995.1032

28. Functional Imaging Laboratory. Statistical parametric mapping. Accessed September 15, 2023. <https://www.fil.ion.ucl.ac.uk/spm/>
29. Davatzikos C, Genc A, Xu D, Resnick SM. Voxel-based morphometry using the RAVENS maps: methods and validation using simulated longitudinal atrophy. *Neuroimage*. 2001;14(6):1361-1369. doi:10.1006/nimg.2001.0937
30. Ostwald D, Schneider S, Bruckner R, Horvath L. Random field theory-based *P* values: a review of the SPM implementation. *arXiv*. Published online August 13, 2018. <http://arxiv.org/abs/1808.04075>.
31. Roweis ST, Saul LK. Nonlinear dimensionality reduction by locally linear embedding. *Science*. 2000;290(5500):2323-2326. doi:10.1126/science.290.5500.2323
32. Zhang Z, Wang J. MLL: modified locally linear embedding using multiple weights. In: Schölkopf B, Platt J, Hoffman T, eds. *Advances in Neural Information Processing Systems*. MIT Press; 2006.
33. Muniz-Terrera G, Hout Av, Rigby RA, Stasinopoulos DM. Analysing cognitive test data: distributions and nonparametric random effects. *Stat Methods Med Res*. 2016;25(2):741-753. doi:10.1177/0962280212465500
34. Liu X. Linear mixed-effects models. In: Liu X, ed. *Methods and Applications of Longitudinal Data Analysis*. Academic Press; 2016:61-94.
35. Benjamini Y, Hochberg Y. Controlling the false discovery rate: a practical and powerful approach to multiple testing. *J R Stat Soc B*. 1995;57(1):289-300. <https://www.jstor.org/stable/2346101> doi:10.1111/j.2517-6161.1995.tb02031.x
36. Davatzikos C, Xu F, An Y, Fan Y, Resnick SM. Longitudinal progression of Alzheimer-like patterns of atrophy in normal older adults: the SPARE-AD index. *Brain*. 2009;132(Pt 8):2026-2035. doi:10.1093/brain/awp091
37. Habes M, Janowitz D, Erus G, et al. Advanced brain aging: relationship with epidemiologic and genetic risk factors, and overlap with Alzheimer disease atrophy patterns. *Transl Psychiatry*. 2016;6(4):e775. doi:10.1038/tp.2016.39
38. Eavani H, Habes M, Satterthwaite TD, et al. Heterogeneity of structural and functional imaging patterns of advanced brain aging revealed via machine learning methods. *Neurobiol Aging*. 2018; 71:41-50. doi:10.1016/j.neurobiolaging.2018.06.013
39. Habes M, Erus G, Toledo JB, et al. White matter hyperintensities and imaging patterns of brain ageing in the general population. *Brain*. 2016;139(Pt 4):1164-1179. doi:10.1093/brain/aww008
40. Kaplan EL, Meier P. Nonparametric estimation from incomplete observations. *J Am Stat Assoc*. 1958;53(282):457-481. doi:10.1080/01621459.1958.10501452
41. Bland JM, Altman DG. The log rank test. *BMJ*. 2004;328(7447):1073. <https://www.ncbi.nlm.nih.gov/pmc/articles/PMC421780/>. doi:10.1136/bmj.328.7447.1073
42. Rand WM. Objective criteria for the evaluation of clustering methods. *J Am Stat Assoc*. 1971;66(336):846-850. doi:10.1080/01621459.1971.10482356
43. Hubert L, Arabie P. Comparing partitions. *J Classif*. 1985;2(1):193-218. doi:10.1007/BF01908075
44. Zhao B, Zhang J, Ibrahim JG, et al. Large-scale GWAS reveals genetic architecture of brain white matter microstructure and genetic overlap with cognitive and mental health traits (n = 17 706). *Mol Psychiatry*. 2021;26(8):3943-3955. doi:10.1038/s41380-019-0569-z
45. van der Meer D, Frei O, Kaufmann T, et al. Understanding the genetic determinants of the brain with MOSTest. *Nat Commun*. 2020;11(1):3512. doi:10.1038/s41467-020-17368-1
46. Persyn E, Hanscombe KB, Howson JMM, Lewis CM, Traylor M, Markus HS. Genome-wide association study of MRI markers of cerebral small vessel disease in 42 310 participants. *Nat Commun*. 2020;11(1):2175. doi:10.1038/s41467-020-15932-3
47. Hoffmann TJ, Ehret GB, Nandakumar P, et al. Genome-wide association analyses using electronic health records identify new loci influencing blood pressure variation. *Nat Genet*. 2017;49(1):54-64. doi:10.1038/ng.3715
48. Coronary Artery Disease (C4D) Genetics Consortium. A genome-wide association study in Europeans and South Asians identifies 5 new loci for coronary artery disease. *Nat Genet*. 2011;43(4):339-344. doi:10.1038/ng.782
49. Gouveia C, Gibbons E, Dehghani N, Eapen J, Guerreiro R, Bras J. Genome-wide association of polygenic risk extremes for Alzheimer disease in the UK Biobank. *Sci Rep*. 2022;12(1):8404. doi:10.1038/s41598-022-12391-2
50. Graham SE, Clarke SL, Wu KHH, et al; VA Million Veteran Program; Global Lipids Genetics Consortium. The power of genetic diversity in genome-wide association studies of lipids. *Nature*. 2021;600(7890):675-679. doi:10.1038/s41586-021-04064-3
51. Richardson TG, Sanderson E, Palmer TM, et al. Evaluating the relationship between circulating lipoprotein lipids and apolipoproteins with risk of coronary heart disease: a multivariable mendelian randomisation analysis. *PLoS Med*. 2020;17(3):e1003062. doi:10.1371/journal.pmed.1003062
52. Stern Y, Barnes CA, Grady C, Jones RN, Raz N. Brain reserve, cognitive reserve, compensation, and maintenance: operationalization, validity, and mechanisms of cognitive resilience. *Neurobiol Aging*. 2019;83:124-129. doi:10.1016/j.neurobiolaging.2019.03.022
53. Muller M, Appelman APA, van der Graaf Y, Vincken KL, Mali WPTM, Geerlings MI. Brain atrophy and cognition: interaction with cerebrovascular pathology? *Neurobiol Aging*. 2011; 32(5):885-893. doi:10.1016/j.neurobiolaging.2009.05.005
54. Attems J, Jellinger KA. The overlap between vascular disease and Alzheimer disease—lessons from pathology. *BMC Med*. 2014;12(1):206. doi:10.1186/s12916-014-0206-2